



Effect of changing NO_x lifetime on the seasonality and long-term trends of satellite-observed tropospheric NO_2 columns over China

Viral Shah¹, Daniel J. Jacob^{1,2}, Ke Li¹, Rachel F. Silvern², Shixian Zhai¹, Mengyao Liu³, Jintai Lin³, and Qiang Zhang⁴

- 5 ¹Harvard John A. Paulson School of Engineering and Applied Sciences, Harvard University, Cambridge, MA, USA.
²Department of Earth and Planetary Sciences, Harvard University, Cambridge, MA, USA.
³Laboratory for Climate and Ocean-Atmosphere Studies, Department of Atmospheric & Oceanic Sciences, School of Physics, Peking University, Beijing, China.
⁴Department of Earth System Science, Tsinghua University, Beijing, China.

10 *Correspondence to:* Viral Shah (vshah@seas.harvard.edu)

Abstract. Satellite observations of tropospheric NO_2 columns are extensively used to infer trends in anthropogenic emissions of nitrogen oxides ($\text{NO}_x \equiv \text{NO} + \text{NO}_2$), but this may be complicated by trends in NO_x lifetime. Here we use 2004–2018 observations from the OMI satellite-based instrument (QA4ECV and POMINO v2 retrievals) to examine the seasonality and trends of tropospheric NO_2 columns over central-eastern China, and we interpret the results with the GEOS-Chem chemical transport model. The observations show a factor of 3 increase in NO_2 columns from summer to winter, which we explain in GEOS-Chem as reflecting a longer NO_x lifetime in winter than in summer (21 h versus 5.9 h in 2017). The 2005–2018 summer trends of OMI NO_2 closely follow the trends in the Multi-resolution Emission Inventory for China (MEIC), with a rise over the 2005–2011 period and a 25% decrease since. We find in GEOS-Chem no significant trend of the NO_x lifetime in summer, supporting the emission trend reported by MEIC. The winter trend of OMI NO_2 is steeper than in summer over the entire period, which we attribute to a decrease in NO_x lifetime at lower NO_x emissions. Half of the NO_x sink in winter is from N_2O_5 hydrolysis, which counterintuitively becomes more efficient as NO_x emissions decrease due to less titration of ozone at night. Formation of organic nitrates also becomes an increasing sink of NO_x as NO_x emissions decrease but emissions of volatile organic compounds (VOCs) do not.

1 Introduction

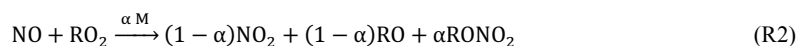
25 Emissions of nitrogen oxides ($\text{NO}_x \equiv \text{NO} + \text{NO}_2$) from fossil fuel combustion in China have been changing fast in the past few decades, due to rapid economic expansion on the one hand and strengthening environmental regulations on the other hand. Growing fossil fuel use with weak pollution controls resulted in almost three-fold increase in China's NO_x emissions between 1990 and 2010, according to bottom-up inventories based on activity data and emission factors (Granier et al., 2011; Zhang et



al., 2012b). Since then, China has adopted strong measures to decrease air pollution by setting stringent emissions standards,
30 capping coal use, increasing vehicle fuel efficiency, closing outdated facilities, and growing renewable energy (Liu et al., 2016;
Zheng et al., 2018). Bottom-up inventories estimate that China's NO_x emissions decreased by 20% between 2011 and 2017,
despite continuing economic expansion (Sun et al., 2018; Zheng et al., 2018). There is a strong need to evaluate these emission
inventories and their trends for air quality management.

Satellite-based observations of tropospheric NO₂ columns by solar backscatter have been used extensively as a proxy for NO_x
35 emissions and their trends (Martin, 2008; Streets et al., 2013). These observations have been qualitatively consistent with the
trends in Chinese NO_x emission inventories, showing an increasing trend of NO₂ columns over China between 1994 and 2011,
and a sharp reversal in eastern China since 2011 (Richter et al., 2005; van der A et al., 2006, 2008; Lin et al., 2010; Krotkov
et al., 2016; Schneider et al., 2015; Duncan et al., 2016; Cui et al., 2016). However, the trends in the NO₂ columns are steeper
40 than in the emission inventories (Zhang et al., 2007; Stavrakou et al., 2008; Zhang et al., 2012b; Hilboll et al., 2013; Liu et al.,
2017; Zheng et al., 2018). For example, Zhang et al. (2007) found that NO₂ columns over China increased two-fold from 1996
to 2004 while their emission inventory reported a 60% increase. For 2010–2015, the Multi-resolution Emission Inventory for
China (MEIC) estimates a 14% decrease in NO_x emissions but NO₂ columns from the OMI satellite instrument indicate a 22%
decrease (Zheng et al., 2018).

Differences in the trends between NO₂ columns and NO_x emission inventories could reflect errors in the inventories (Saikawa
45 et al., 2017) and satellite retrievals (Lin et al., 2014; Lorente et al., 2017), but also trends in the lifetime of NO_x against
atmospheric oxidation. This lifetime is of the order of hours and may change with the chemical environment, including the
NO_x concentration itself (Stavrakou et al., 2008; Lamsal et al., 2011; Valin et al., 2011; Lu and Streets, 2012; Duncan et al.,
2013; Gu et al., 2016; Cooper et al., 2017; Laughner and Cohen, 2019). NO_x is oxidized to nitric acid (HNO₃) and organic
nitrates (RONO₂), including peroxyacyl nitrates (RC(O)OONO₂). There is also a minor sink from NO₂ dry deposition (Zhang
50 et al., 2012a). Oxidation in the daytime is driven by photochemically produced hydrogen oxide (HO_x≡OH+HO₂+RO₂)
radicals:

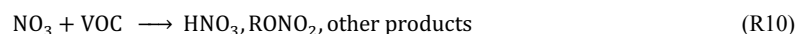
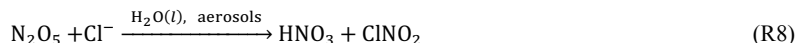
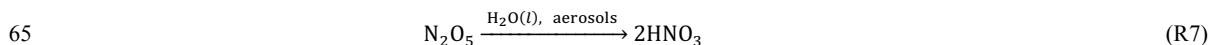


55 NO_x and HO_x concentrations are tightly interlinked (Kleinman, 1994; Laughner and Cohen, 2019). When NO_x levels are
sufficiently low (the so-called NO_x-limited conditions), an increase in NO_x drives an increase in HO_x, particularly OH through

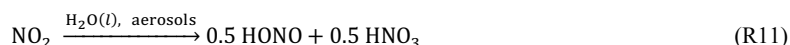


the $\text{NO} + \text{HO}_2 \rightarrow \text{NO}_2 + \text{OH}$ reaction. When NO_x levels are high (the so-called NO_x -saturated conditions), reaction R1 becomes the dominant HO_x sink and an increase in NO_x causes a decrease in HO_x .

At night, the chemical loss of NO_x proceeds through a series of reactions (R4–R10) beginning with the oxidation of NO and NO_2 by O_3 to form nitrate radical (NO_3) and dinitrogen pentoxide (N_2O_5). N_2O_5 and NO_3 react in aerosols to produce HNO_3 , and NO_3 additionally reacts with volatile organic compounds (VOCs) to form either HNO_3 or RONO_2 :



A change in NO_x emissions can change the nighttime levels of ozone and reaction (R6) is quadratic in NO_x concentrations, leading to nonlinearity between NO_x emissions and NO_2 concentrations. In addition, aerosol concentrations in China have decreased by about 30% since 2013 (Lin et al., 2018; Zheng et al., 2018; Zhai et al., 2019), which would decrease the rate of nighttime NO_x loss (R7–R9). A decrease in aerosol concentrations will also slow the NO_x loss by hydrolysis of NO_2 in aerosols:



Here we present trends in tropospheric NO_2 columns over China from 2004 to 2018 observed by the Ozone Monitoring Instrument (OMI) satellite instrument, showing a peak in 2011. We use the GEOS-Chem chemical transport model applied to the MEIC inventory (Zheng et al., 2018) to investigate how changes in NO_x lifetimes have affected the relationship between tropospheric NO_2 columns and NO_x emissions, and whether this can reconcile the differences in trends between the two quantities. Results have important implications for the use of satellite NO_2 retrievals to infer trends in NO_x emissions.



2 Observations and model

80 2.1 OMI NO₂ column retrievals

We use 2004–2018 tropospheric NO₂ column data retrieved from the OMI instrument aboard the NASA Aura satellite. Aura is in sun-synchronous polar orbit satellite with daytime equator crossing at 13:45 local solar time (LST). OMI measures backscattered solar radiation from the Earth in the ultraviolet and visible wavelength range (270–504 nm). It has a swath width of 2600 km and a ground pixel size of 13 km × 24 km at nadir (Levelt et al., 2006, 2018). Several OMI pixels are affected by the so-called row anomaly possibly from an obstruction in their field of view (Dobber et al., 2008). Pixels not affected by the row anomaly have no significant calibration drift over the length of the record (Boersma et al., 2018).

We use tropospheric NO₂ columns from two retrievals: the European Quality Assurance for Essential Climate Variables (QA4ECV) project's NO₂ ECV precursor product (Boersma et al., 2018) and the Peking University POMINO product, version 2 (Lin et al., 2015; Liu et al., 2019). NO₂ tropospheric column retrieval in the ECV product involves (1) spectral fit of the backscattered solar radiation in the 405–465 nm window to obtain the total NO₂ slant column (SC), (2) removal of the stratospheric component by data assimilation with the TM5-MP chemical transport model, and (3) conversion of the tropospheric SC to a tropospheric vertical column (VC) with an air mass factor (AMF = SC/VC) that depends on viewing geometry, surface albedo, retrieved cloud properties, and the NO₂ vertical profile (taken from the TM5-MP model).

The POMINO v2 product starts with the tropospheric NO₂ slant columns from the ECV retrieval but uses different methods and data sources for the AMF calculation. The main difference is the treatment of aerosols. ECV assumes that aerosol effects are implicitly accounted for in the independent retrieval of cloud pressure and cloud fraction, which are prerequisites for NO₂ retrievals. POMINO explicitly accounts for aerosols in the radiative transfer calculations with aerosol optical properties and vertical profiles from the GEOS-Chem model corrected with satellite observations from the MODIS and CALIOP instruments. In polluted areas (aerosol optical depth greater than 0.5), the choice of aerosol correction method can affect the AMF by 45% (Lorente et al., 2017) and the sign of the correction depends on the vertical distribution of aerosols relative to NO₂ (Palmer et al., 2001; Martin et al., 2003; Liu et al., 2019). POMINO also includes angular dependence of surface reflectance, online radiative transfer calculation, and consistency in retrievals of cloud properties and NO₂ (Lin et al., 2015; Liu et al., 2019).

We create monthly mean gridded (0.5° latitude × 0.625° longitude) datasets of ECV and POMINO NO₂ columns over China for June-July-August (JJA) 2005–2018 and December-January-February (DJF) 2004–2018. We exclude pixels with snow-covered surfaces and cloud fraction greater than 30%. We use cloud fraction data from the corresponding retrievals. We include only cross-track viewing positions of 5 through 22 to exclude data affected by the row anomaly (Boersma et al., 2018) and swath edges. For comparison with GEOS-Chem, the POMINO and ECV NO₂ columns are recalculated with modified air mass factors using the pixel-specific GEOS-Chem NO₂ vertical profiles (Palmer et al., 2001).



2.2 Ground-based observations

110 We use hourly measurements of NO_2 and O_3 concentrations from the network of ~ 1000 sites operated by the China Ministry of Ecology and Environment (MEE) since 2013 (<http://beijingair.sinaapp.com>). We correct the known interference of organic nitrates and HNO_3 in the NO_2 measurements by using the GEOS-Chem simulated concentrations for those species following Lamsal et al. (2008). We then grid ($0.5^\circ \times 0.625^\circ$ grid) and seasonally average the data, discarding sites with less than 50% coverage in a season.

115 2.3 GEOS-Chem model

We use the GEOS-Chem chemical transport model version 12.1.0 (www.geos-chem.org) driven by assimilated meteorological fields from the NASA Global Modeling and Assimilation Office's Modern-Era Retrospective analysis for Research and Applications, version 2 (MERRA-2) system (Gelaro et al., 2017). GEOS-Chem simulates the chemistry of major gas- and aerosol-phase species in the troposphere (Pye et al., 2009; Kim et al., 2015; Travis et al., 2016; Fisher et al., 2016; Sherwen et al., 2016). We use the GEOS-Chem Classic nested-grid configuration over East Asia (11°S – 55°N , 60 – 150°E) at $0.5^\circ \times 0.625^\circ$ resolution (Wang et al., 2004; Chen et al., 2009), with lateral chemical boundary conditions from a $4^\circ \times 5^\circ$ global simulation. Anthropogenic emissions over China are from the MEIC inventory updated annually for 2000–2017 (www.meicmodel.org; Zheng et al., 2018). MEIC includes monthly emission profiles for each sector (Li et al., 2017a) and hourly profiles developed at Tsinghua University. We vertically resolve emissions from point sources (power plants and industries) following profiles used in the LOTOS-EUROS model (Manders et al., 2017), and speciate anthropogenic NO_x emissions as NO (90%), NO_2 (9.2%) and HONO (0.8%) following Menut et al. (2013). GEOS-Chem includes additional NO_x emissions from soil and fertilizer use (Hudman et al., 2012), lightning (Murray et al., 2012), shipping (Vinken et al., 2011; Holmes et al., 2014) and aircraft (Stettler et al., 2011). Vertical mixing in the planetary boundary layer is simulated using a non-local mixing scheme (Lin and McElroy, 2010).

130 We modified the standard GEOS-Chem version 12.1.0 chemistry to update the reactive uptake coefficients (γ) of N_2O_5 , NO_3 , and NO_2 on aerosols (Jacob, 2000) based on recent comparison of GEOS-Chem to observations from the Wintertime Investigation of Transport, Emissions, and Reactivity (WINTER) aircraft campaign over the eastern United States (Jaeglé et al., 2018; Shah et al., 2018). $\gamma_{\text{N}_2\text{O}_5}$ is computed following Bertram and Thornton (2009) for sulfate-nitrate-ammonium aerosols, and is taken to be 1×10^{-4} ($\text{RH} < 50\%$) or 1×10^{-3} ($\text{RH} > 50\%$) for organic aerosols. γ_{NO_3} is taken to be 1×10^{-3} following Jacob (2000). γ_{NO_2} for the hydrolysis reaction (R11) is decreased from 1×10^{-4} to 1×10^{-5} on the basis of laboratory measurements (Bröske et al., 2003; Stemmler et al., 2007; Tan et al., 2016). This decrease of γ_{NO_2} yields a 24 h mean wintertime HONO/ NO_2 molar concentration ratio of 0.035 over eastern China in GEOS-Chem, consistent with the observed range of 0.015–0.071 (Hendrick et al., 2014; Spataro et al., 2013; Wang et al., 2017, 2013).



We evaluate the model with the spatial and seasonal distributions of OMI NO₂ observations for 2016/17 DJF and 2017 JJA
140 (the latest year with MEIC data) and use these two periods to analyze the seasonality of NO_x lifetime and loss pathways in the
model. To calculate the emission-driven changes in NO_x lifetimes, we conduct a sensitivity simulation in which we set
anthropogenic emissions over China to 2012 levels but use the 2016/17 meteorology and NO_x emissions from soils, lightning,
ships, and aircraft. Chinese NO_x emissions decreased by 25% from 2012 to 2017 according to MEIC (Supplement Fig. S1).
For comparison with OMI observations, we sample the model at 13–14 LST and exclude model columns with surface snow
145 cover or with model cloud fraction greater than 30%. We focus on the large polluted region of central-eastern China (30–41°N,
112–122°E; rectangle in left panels of Fig. 1), where we may expect tropospheric NO₂ columns to be most sensitive to Chinese
NO_x emissions, and where the relatively narrow latitude range leads to consistent seasonal variations. This region accounted
for 50% of anthropogenic Chinese emissions in 2017 according to MEIC.

3 Results and discussion

150 3.1 Seasonal variation of NO₂ columns and NO_x lifetimes

Figure 1 shows the NO₂ columns from the POMINO and ECV retrievals, and from the GEOS-Chem model, for JJA 2017 and
DJF 2016/17. In central-eastern China, we find that in both seasons over 70% of the GEOS-Chem tropospheric NO₂ column
as would be observed by OMI is in the boundary layer below 2 km altitude. Thus we expect the NO₂ column to reflect mostly
the local NO_x emissions rather than the free tropospheric background (Silvern et al., 2019). In summer, average GEOS-Chem
155 NO₂ columns over central-eastern China are within 10% of the POMINO and ECV NO₂ columns. There is scatter in the spatial
relationship ($r \approx 0.5$) that could be due to a combination of model and retrieval errors. In winter, however, POMINO is 42%
higher than GEOS-Chem while ECV is 16% lower. The difference in aerosol correction between POMINO and ECV is largest
in winter, due to high aerosol concentrations and high solar zenith angles. In ECV, polluted scenes with high aerosol optical
depths (and likely high NO₂) can be misclassified as cloudy and excluded from the seasonal-mean, which leads to a negative
160 sampling bias (Lin et al., 2014, 2015; Liu et al., 2019). On the other hand, retrieving NO₂ columns under high-aerosol
conditions can be uncertain because of the strong sensitivity to the vertical distribution of NO₂ relative to that of aerosols,
although this is less of a problem in POMINO as it uses the CALIOP-observed aerosol vertical profiles (Lin et al., 2014, 2015;
Liu et al., 2019).

Liu et al. (2019) compared the ECV and POMINO retrievals to ground-based Multi Axis Differential Optical Absorption
165 Spectroscopy (MAX-DOAS) NO₂ column observations on 49 days in 3 Chinese cities. POMINO was on average closer to the
MAX-DOAS NO₂ than ECV (-3% versus -22% bias) and on hazy days (+4% versus -26% bias), but on clear (cloud fraction=0)
days ECV performed better (-6% bias) than POMINO (+30% bias). These biases were slightly larger in fall and winter,
although sampling in individual seasons was sparse. There is uncertainty in the comparison as the column observed by MAX-



DOAS may not be representative of the satellite pixel, and aerosol vertical profiles used in the satellite and MAX-DOAS
170 retrievals may be inconsistent (Lin et al., 2014).

Figure 2 compares the mean winter-summer ratios of NO_2 columns from the ECV and POMINO retrievals over central-eastern
China with GEOS-Chem and with the ratios of 24 h mean surface NO_2 concentrations at the MEE sites. GEOS-Chem shows
similar ratios for NO_2 columns and surface NO_2 , as would be expected since most of the tropospheric NO_2 column is in the
boundary layer. We find that the seasonal amplitude in the MEE data is most consistent with the ECV NO_2 columns, whereas
175 the seasonal amplitude of POMINO NO_2 is larger. Winter-summer ratios of NO_2 columns are 2.6 in the ECV retrieval, 3.5 in
POMINO, and 2.7 in GEOS-Chem. Winter-summer ratios of surface NO_2 concentrations are 2.3 in the MEE data and 2.5 in
GEOS-Chem. Anthropogenic NO_x emissions in the MEIC inventory peak in winter but the winter-summer ratio is only 1.15
(Li et al., 2017b). We find in GEOS-Chem that the seasonal variation in NO_2 columns is mainly driven by the NO_x lifetime in
the boundary layer, which increases from 5.9 h in summer to 21 h in winter for 2017 (Fig. 3). In summer, NO_x is lost mostly
180 through oxidation by OH in daytime (43%) and through N_2O_5 hydrolysis at night (33%). In winter, the NO_x lifetime is much
longer because of the lower concentrations of OH and RO_2 radicals. N_2O_5 hydrolysis accounts for 51% of NO_x loss in winter.
Remarkably, the loss of NO_x from N_2O_5 hydrolysis is a factor of 2 slower in winter than in summer, despite the longer nights
and higher aerosol concentrations (Zhai et al., 2019), because of the low nighttime ozone concentrations. The overall NO_x
lifetime in winter and the contribution from N_2O_5 hydrolysis are similar to values inferred over the eastern US during the
185 WINTER campaign (Jaeglé et al., 2018), despite a factor of ~ 5 difference in aerosol concentrations between the two regions.
Loss of NO_x by N_2O_5 hydrolysis in China in winter is limited by the supply of ozone, not the supply of aerosol.

Leue et al. (2001) previously estimated the NO_x lifetime in the eastern US by using the offshore gradient of satellite-observed
 NO_2 columns. We tried this approach and found that the offshore gradients of NO_2 columns perpendicular to the east coast of
China are consistent between model and observations (Fig. 4). However, there is little seasonal difference in the gradients,
190 suggesting that their magnitudes are determined by dilution more than chemical decay.

3.2 2004–2018 trends in NO_2 columns and lifetimes

Figure 5 shows the trends in the summer and winter NO_2 columns from the ECV retrieval, and in anthropogenic NO_x emissions
from MEIC, over central-eastern China for the 2004–2018 extent of the OMI record. According to MEIC, NO_x emissions
increased at 5–6% a^{-1} in 2005–2011 and decreased at the same pace after 2011. OMI NO_2 columns mirror the trajectory of the
195 MEIC NO_x emissions: rising between 2005 and 2011, reversing direction in 2011/12, and falling back to around 2005 levels
by 2018. The summer trends in OMI NO_2 closely track the MEIC emissions but the winter trends are steeper. The same
summer-winter differences in NO_2 column trends over China are seen in the POMINO retrieval (Supplement Fig. S2) and in
retrievals from the Ozone Mapping Profiler Suite (OMPS) instrument (Lin et al., 2019). Previous studies also reported such a



seasonal difference between summer and winter NO₂ column trends (Uno et al., 2007; Zhang et al., 2007; Stavrou et al.,
200 2008; Gu et al., 2013).

The steeper slopes in winter could reflect a trend in NO_x lifetime as NO_x and other emissions change. A few modeling studies
have previously explored this dependence for China. Uno et al. (2007) found no significant change in the annual mean NO_x
lifetime over 1996–2004. Stavrou et al. (2008) found that the increase in NO_x emissions over 1997–2006 drove a 25%
decrease in summer NO_x lifetime, due to higher OH from faster NO+HO₂ reaction, and a 10% increase in winter NO_x lifetime,
205 due to lower OH from faster NO₂+OH reaction.

We examined the effect of 2012–2017 changes in MEIC emissions for NO_x and other species on the lifetime of NO_x simulated
by GEOS-Chem (Fig. 3). During that period, NO_x emissions in central-eastern China decreased by 25% and boundary layer
aerosol concentrations in GEOS-Chem decreased by 20%. Observed aerosol concentrations from the MEE network decreased
by 30% over the 2013–2017 period (Zhai et al., 2019). We find no significant change in the summer NO_x lifetime between
210 2012 and 2017. The NO_x lifetime during the day shortened slightly, as summertime OH concentrations increased by 6% and
RO₂ concentrations increased by 13%. However, the NO_x lifetime during the night increased as aerosol concentrations dropped,
canceling the overall effect.

In contrast, the winter NO_x lifetime decreased by 22% (from 27 to 21 h) between 2012 and 2017 (Fig. 3), driven mostly by
faster loss by N₂O₅ hydrolysis in aerosols, and also by faster loss from reactions with OH and RO₂. The loss rate from RO₂ +
215 NO/NO₂ is largely determined by the emission rate of VOCs, which changed by less than 3% over 2012–2017 (Zheng et al.,
2018), effectively decreasing the NO_x lifetime as NO_x emissions dropped. The faster loss by N₂O₅ hydrolysis might seem
counterintuitive since both aerosols and NO_x dropped over the period. However, winter aerosol levels for converting N₂O₅ to
HNO₃ remain in excess even in 2017. Instead, we find that the driving factor behind the increase in N₂O₅ hydrolysis is a rise
in nighttime ozone concentrations. At night, fast titration by NO (reaction R4) is an important sink of ozone close to NO_x
220 sources. As NO_x emissions decrease, less ozone is titrated, which then enables the formation of NO₃ by reaction (R5) and
subsequent formation of N₂O₅. The simulated NO_x lifetime against loss by N₂O₅ hydrolysis decreases by 26% from 54 h in the
winter 2011/12 to 40 h in the winter 2016/17. Ground-based observations at the MEE sites show an increase in winter nighttime
ozone consistent with the model (Fig. 6).

Figure 5 shows the implications of these changes in seasonal NO_x lifetime on the 2012–2017 NO₂ column trends simulated by
225 GEOS-Chem. There is no significant change in NO_x lifetime in summer and therefore the NO₂ columns track the MEIC
emission trends, consistent with observations. In winter, the shortening of the NO_x lifetime steepens the trends of NO₂ columns
relative to NO_x emissions. Wintertime GEOS-Chem NO₂ columns decrease by 35% between 2011/12 and 2016/17, faster than
the 25% decrease in the MEIC NO_x emissions. The NO_x lifetime in winter is about one day, long enough for faster NO_x loss



at night to affect NO_2 columns in the afternoon when OMI makes its observations. Comparison to the observed wintertime
230 trend suggests that the GEOS-Chem decrease in NO_x lifetime over 2012–2017 may not be steep enough. There is substantial
uncertainty in the factors controlling wintertime OH concentrations (Tan et al., 2018; Miao et al., 2018) and these might also
affect the model trend. Meteorological variability can also cause interannual changes in wintertime NO_2 of ~20% (Lin and
McElroy, 2011), but the effect on longer-term trends will be smaller. GEOS-Chem trends for 2005–2012 should be symmetric
to those for 2012–2017, since NO_x emissions in 2005 are similar to those in 2017 (Fig. 5).

235 The use of satellite-based NO_2 column observations to evaluate trends in NO_x emission inventories in China can be compared
to similar work previously done for the US. Jiang et al. (2018) found that OMI NO_2 columns over the US during 2009–2015
decreased slower than NO_x emissions in the US Environment Protection Agency's (EPA) National Emissions Inventory (NEI),
suggesting that NO_x emission controls were not as effective as reported by the NEI. However, Silvern et al. (2019) explained
this discrepancy by a large relative contribution of the free tropospheric background to the NO_2 column over the US, weakening
240 the relationship between NO_2 columns and US anthropogenic NO_x emissions. This is not a major concern over central-eastern
China, where the contribution of the free troposphere above 2 km to the tropospheric NO_2 column as sensed by OMI is less
than 30%. Laughner & Cohen (2019) find an increase in summer NO_x lifetime over 2010–2013 in OMI observations of isolated
urban plumes over the US, reflecting NO_x -limited conditions where OH concentrations decrease as NO_x decreases. This would
dampen the response of NO_2 columns to emission reductions. Such an effect is not apparent in central-eastern China, which is
245 prevailing in the so-called transition regime between NO_x -saturated and NO_x -limited conditions (Jin and Holloway, 2015;
Li et al., 2019).

4 Conclusions

We examined the seasonality and trends of satellite-derived tropospheric NO_2 columns over China and their relation to NO_x
emissions. Observations from the satellite-based OMI instrument show a factor of 3 increase in tropospheric NO_2 columns
250 from summer to winter, and we show that this can be explained by the seasonal variation in NO_x lifetime against oxidation.
 NO_2 columns for the 2004–2018 duration of the OMI record peak in 2011 and subsequently decrease, consistent with the
Multi-resolution Emission Inventory for China (MEIC). The summer trends in OMI NO_2 columns match closely the MEIC
emission trends, but the winter trends are steeper than MEIC. We attribute the steeper winter trends to a decrease in the NO_x
lifetime, mostly by faster N_2O_5 hydrolysis in aerosols, as NO_x emissions decrease. Lower NO_x emissions lead to an increase
255 in nighttime ozone in winter, promoting N_2O_5 formation. Our analysis of the OMI NO_2 column observations thus supports the
magnitude and trends of NO_x emissions in the MEIC inventory, while emphasizing the need to account for changes in NO_x
lifetime when interpreting trends in satellite NO_2 columns in terms of trends in NO_x emissions.



Data availability. The QA4ECV data is available at <http://www.qa4ecv.eu>, POMINO v2 at
260 <http://www.phy.pku.edu.cn/~acm/acmProduct.php#POMINO>, the MEE surface data at <http://beijingair.sinaapp.com> and the
MEIC inventory data at <http://www.meicmodel.org>. GEOS-Chem results are available on request from the corresponding
author.

Author contributions. VS and DJJ designed the study. VS performed the model simulations and data analysis. KL and SZ
processed the ground-based observations. RFS contributed analysis software. ML and JL provided the POMINO data. QZ
265 provided the MEIC data. VS and DJJ wrote the paper with contributions from all co-authors.

Competing interests. The authors declare that they have no conflict of interest.

Acknowledgments. This work was funded by the NASA Earth Science Division. The development of POMINO product was
funded by the National Natural Science Foundation of China (41775115). We acknowledge the QA4ECV project for the NO₂
data.

270 References

- Boersma, K. F., Eskes, H. J., Richter, A., De Smedt, I., Lorente, A., Beirle, S., van Geffen, J. H. G. M., Zara, M., Peters, E.,
Van Roozendaal, M., Wagner, T., Maasackers, J. D., van der A, R. J., Nightingale, J., De Rudder, A., Irie, H., Pinardi, G.,
Lambert, J.-C. and Compernelle, S. C.: Improving algorithms and uncertainty estimates for satellite NO₂ retrievals: results
275 from the quality assurance for the essential climate variables (QA4ECV) project, *Atmospheric Measurement Techniques*,
11(12), 6651–6678, doi:10.5194/amt-11-6651-2018, 2018.
- Bröske, R., Kleffmann, J. and Wiesen, P.: Heterogeneous conversion of NO₂ on secondary organic aerosol surfaces: A possible
source of nitrous acid (HONO) in the atmosphere?, *Atmospheric Chemistry and Physics*, 3(3), 469–474, doi:10.5194/acp-3-
469-2003, 2003.
- Chen, D., Wang, Y., McElroy, M. B., He, K., Yantosca, R. M. and Le Sager, P.: Regional CO pollution and export in China
280 simulated by the high-resolution nested-grid GEOS-Chem model, *Atmospheric Chemistry and Physics*, 9(11), 3825–3839,
doi:10.5194/acp-9-3825-2009, 2009.
- Cooper, M., Martin, R. V., Padmanabhan, A. and Henze, D. K.: Comparing mass balance and adjoint methods for inverse
modeling of nitrogen dioxide columns for global nitrogen oxide emissions, *Journal of Geophysical Research: Atmospheres*,
122(8), 4718–4734, doi:10.1002/2016JD025985, 2017.
- 285 Cui, Y., Lin, J., Song, C., Liu, M., Yan, Y., Xu, Y. and Huang, B.: Rapid growth in nitrogen dioxide pollution over Western
China, 2005–2013, *Atmospheric Chemistry and Physics*, 16(10), 6207–6221, doi:10.5194/acp-16-6207-2016, 2016.



- Dobber, M., Voors, R., Dirksen, R., Kleipool, Q. and Levelt, P.: The High-Resolution Solar Reference Spectrum between 250 and 550 nm and its Application to Measurements with the Ozone Monitoring Instrument, *Solar Physics*, 249(2), 281–291, doi:10.1007/s11207-008-9187-7, 2008.
- 290 Duncan, B. N., Yoshida, Y., de Foy, B., Lamsal, L. N., Streets, D. G., Lu, Z., Pickering, K. E. and Krotkov, N. A.: The observed response of Ozone Monitoring Instrument (OMI) NO₂ columns to NO_x emission controls on power plants in the United States: 2005–2011, *Atmospheric Environment*, 81, 102–111, doi:10.1016/j.atmosenv.2013.08.068, 2013.
- Duncan, B. N., Lamsal, L. N., Thompson, A. M., Yoshida, Y., Lu, Z., Streets, D. G., Hurwitz, M. M. and Pickering, K. E.: A space-based, high-resolution view of notable changes in urban NO_x pollution around the world (2005–2014), *Journal of Geophysical Research: Atmospheres*, 121(2), 976–996, doi:10.1002/2015JD024121, 2016.
- 295 Fisher, J. A., Jacob, D. J., Travis, K. R., Kim, P. S., Marais, E. A., Chan Miller, C., Yu, K., Zhu, L., Yantosca, R. M., Sulprizio, M. P., Mao, J., Wennberg, P. O., Crouse, J. D., Teng, A. P., Nguyen, T. B., St. Clair, J. M., Cohen, R. C., Romer, P., Nault, B. A., Wooldridge, P. J., Jimenez, J. L., Campuzano-Jost, P., Day, D. A., Hu, W., Shepson, P. B., Xiong, F., Blake, D. R., Goldstein, A. H., Misztal, P. K., Hanisco, T. F., Wolfe, G. M., Ryerson, T. B., Wisthaler, A. and Mikoviny, T.: Organic nitrate chemistry and its implications for nitrogen budgets in an isoprene- and monoterpene-rich atmosphere: constraints from aircraft (SEAC⁴RS) and ground-based (SOAS) observations in the Southeast US, *Atmospheric Chemistry and Physics*, 16(9), 5969–5991, doi:10.5194/acp-16-5969-2016, 2016.
- 300 Gelaro, R., McCarty, W., Suárez, M. J., Todling, R., Molod, A., Takacs, L., Randles, C. A., Darmenov, A., Bosilovich, M. G., Reichle, R., Wargan, K., Coy, L., Cullather, R., Draper, C., Akella, S., Buchard, V., Conaty, A., da Silva, A. M., Gu, W., Kim, G.-K., Koster, R., Lucchesi, R., Merkova, D., Nielsen, J. E., Partyka, G., Pawson, S., Putman, W., Rienecker, M., Schubert, S. D., Sienkiewicz, M. and Zhao, B.: The Modern-Era Retrospective Analysis for Research and Applications, Version 2 (MERRA-2), *J. Climate*, 30(14), 5419–5454, doi:10.1175/JCLI-D-16-0758.1, 2017.
- 305 Granier, C., Bessagnet, B., Bond, T., D'Angiola, A., Denier van der Gon, H., Frost, G. J., Heil, A., Kaiser, J. W., Kinne, S., Klimont, Z., Kloster, S., Lamarque, J.-F., Liousse, C., Masui, T., Meleux, F., Mieville, A., Ohara, T., Raut, J.-C., Riahi, K., Schultz, M. G., Smith, S. J., Thompson, A., van Aardenne, J., van der Werf, G. R. and van Vuuren, D. P.: Evolution of anthropogenic and biomass burning emissions of air pollutants at global and regional scales during the 1980–2010 period, *Climatic Change*, 109(1), 163, doi:10.1007/s10584-011-0154-1, 2011.
- 310 Gu, D., Wang, Y., Smeltzer, C. and Liu, Z.: Reduction in NO_x Emission Trends over China: Regional and Seasonal Variations, *Environmental Science & Technology*, 47(22), 12912–12919, doi:10.1021/es401727e, 2013.
- 315 Gu, D., Wang, Y., Yin, R., Zhang, Y. and Smeltzer, C.: Inverse modelling of NO_x emissions over eastern China: uncertainties due to chemical non-linearity, *Atmospheric Measurement Techniques*, 9(10), 5193–5201, doi:10.5194/amt-9-5193-2016, 2016.
- 320 Hendrick, F., Müller, J.-F., Clémer, K., Wang, P., De Mazière, M., Fayt, C., Gielen, C., Hermans, C., Ma, J. Z., Pinardi, G., Stavrakou, T., Vlemmix, T. and Van Roozendaal, M.: Four years of ground-based MAX-DOAS observations of HONO and NO₂ in the Beijing area, *Atmospheric Chemistry and Physics*, 14(2), 765–781, doi:10.5194/acp-14-765-2014, 2014.
- Hilboll, A., Richter, A. and Burrows, J. P.: Long-term changes of tropospheric NO₂ over megacities derived from multiple satellite instruments, *Atmospheric Chemistry and Physics*, 13(8), 4145–4169, doi:10.5194/acp-13-4145-2013, 2013.



- 325 Holmes, C. D., Prather, M. J. and Vinken, G. C. M.: The climate impact of ship NO_x emissions: an improved estimate accounting for plume chemistry, *Atmospheric Chemistry and Physics*, 14(13), 6801–6812, doi:10.5194/acp-14-6801-2014, 2014.
- Hudman, R. C., Moore, N. E., Mebust, A. K., Martin, R. V., Russell, A. R., Valin, L. C. and Cohen, R. C.: Steps towards a mechanistic model of global soil nitric oxide emissions: implementation and space based-constraints, *Atmospheric Chemistry and Physics*, 12(16), 7779–7795, doi:10.5194/acp-12-7779-2012, 2012.
- 330 Jacob, D.: Heterogeneous chemistry and tropospheric ozone, *Atmospheric Environment*, 34(12–14), 2131–2159, doi:10.1016/S1352-2310(99)00462-8, 2000.
- Jaeglé, L., Shah, V., Thornton, J. A., Lopez-Hilfiker, F. D., Lee, B. H., McDuffie, E. E., Fibiger, D., Brown, S. S., Veres, P., Sparks, T. L., Ebben, C. J., Wooldridge, P. J., Kenagy, H. S., Cohen, R. C., Weinheimer, A. J., Campos, T. L., Montzka, D. D., Digangi, J. P., Wolfe, G. M., Hanisco, T., Schroder, J. C., Campuzano-Jost, P., Day, D. A., Jimenez, J. L., Sullivan, A. P., Guo, H. and Weber, R. J.: Nitrogen Oxides Emissions, Chemistry, Deposition, and Export Over the Northeast United States
335 During the WINTER Aircraft Campaign, *Journal of Geophysical Research: Atmospheres*, 123(21), 12,368–12,393, doi:10.1029/2018JD029133, 2018.
- Jiang, Z., McDonald, B. C., Worden, H., Worden, J. R., Miyazaki, K., Qu, Z., Henze, D. K., Jones, D. B. A., Arellano, A. F., Fischer, E. V., Zhu, L. and Boersma, K. F.: Unexpected slowdown of US pollutant emission reduction in the past decade, *Proceedings of the National Academy of Sciences*, 115(20), 5099, doi:10.1073/pnas.1801191115, 2018.
- 340 Jin, X. and Holloway, T.: Spatial and temporal variability of ozone sensitivity over China observed from the Ozone Monitoring Instrument, *Journal of Geophysical Research: Atmospheres*, 120(14), 7229–7246, doi:10.1002/2015JD023250, 2015.
- Kim, P. S., Jacob, D. J., Fisher, J. A., Travis, K., Yu, K., Zhu, L., Yantosca, R. M., Sulprizio, M. P., Jimenez, J. L., Campuzano-Jost, P., Froyd, K. D., Liao, J., Hair, J. W., Fenn, M. A., Butler, C. F., Wagner, N. L., Gordon, T. D., Welti, A., Wennberg, P. O., Crounse, J. D., St. Clair, J. M., Teng, A. P., Millet, D. B., Schwarz, J. P., Markovic, M. Z. and Perring, A. E.: Sources,
345 seasonality, and trends of southeast US aerosol: an integrated analysis of surface, aircraft, and satellite observations with the GEOS-Chem chemical transport model, *Atmospheric Chemistry and Physics*, 15(18), 10411–10433, doi:10.5194/acp-15-10411-2015, 2015.
- Kleinman, L.: Low and high NO_x tropospheric photochemistry, *Journal of Geophysical Research: Atmospheres*, 99(D8), 16831–16838, doi:10.1029/94JD01028, 1994.
- 350 Krotkov, N. A., McLinden, C. A., Li, C., Lamsal, L. N., Celarier, E. A., Marchenko, S. V., Swartz, W. H., Bucsela, E. J., Joiner, J., Duncan, B. N., Boersma, K. F., Veeckind, J. P., Levelt, P. F., Fioletov, V. E., Dickerson, R. R., He, H., Lu, Z. and Streets, D. G.: Aura OMI observations of regional SO₂ and NO₂ pollution changes from 2005 to 2015, *Atmospheric Chemistry and Physics*, 16(7), 4605–4629, doi:10.5194/acp-16-4605-2016, 2016.
- Lamsal, L. N., Martin, R. V., van Donkelaar, A., Steinbacher, M., Celarier, E. A., Bucsela, E., Dunlea, E. J. and Pinto, J. P.:
355 Ground-level nitrogen dioxide concentrations inferred from the satellite-borne Ozone Monitoring Instrument, *Journal of Geophysical Research: Atmospheres*, 113(D16), doi:10.1029/2007JD009235, 2008.
- Lamsal, L. N., Martin, R. V., Padmanabhan, A., van Donkelaar, A., Zhang, Q., Sioris, C. E., Chance, K., Kurosu, T. P. and Newchurch, M. J.: Application of satellite observations for timely updates to global anthropogenic NO_x emission inventories, *Geophysical Research Letters*, 38(5), doi:10.1029/2010GL046476, 2011.



- 360 Laughner, J. L. and Cohen, R. C.: Direct observation of changing NO_x lifetime in North American cities, in review, 2019.
- Leue, C., Wenig, M., Wagner, T., Klimm, O., Platt, U. and Jähne, B.: Quantitative analysis of NO_x emissions from Global Ozone Monitoring Experiment satellite image sequences, *Journal of Geophysical Research: Atmospheres*, 106(D6), 5493–5505, doi:10.1029/2000JD900572, 2001.
- 365 Levelt, P. F., Oord, G. H. J. van den, Dobber, M. R., Malkki, A., and Stammes, P., Lundell, J. O. V. and Saari, H.: The ozone monitoring instrument, *IEEE Transactions on Geoscience and Remote Sensing*, 44(5), 1093–1101, doi:10.1109/TGRS.2006.872333, 2006.
- Levelt, P. F., Joiner, J., Tamminen, J., Veefkind, J. P., Bhartia, P. K., Stein Zweers, D. C., Duncan, B. N., Streets, D. G., Eskes, H., van der A, R., McLinden, C., Fioletov, V., Carn, S., de Laat, J., DeLand, M., Marchenko, S., McPeters, R., Ziemke, J., Fu, D., Liu, X., Pickering, K., Apituley, A., González Abad, G., Arola, A., Boersma, F., Chan Miller, C., Chance, K., de Graaf, M., Hakkarainen, J., Hassinen, S., Ialongo, I., Kleipool, Q., Krotkov, N., Li, C., Lamsal, L., Newman, P., Nowlan, C., Suleiman, R., Tilstra, L. G., Torres, O., Wang, H. and Wargan, K.: The Ozone Monitoring Instrument: overview of 14 years in space, *Atmospheric Chemistry and Physics*, 18(8), 5699–5745, doi:10.5194/acp-18-5699-2018, 2018.
- 370 Li, K., Jacob, D. J., Liao, H., Shen, L., Zhang, Q. and Bates, K. H.: Anthropogenic drivers of 2013–2017 trends in summer surface ozone in China, *Proceedings of the National Academy of Sciences*, 116(2), 422, doi:10.1073/pnas.1812168116, 2019.
- 375 Li, M., Liu, H., Geng, G., Hong, C., Liu, F., Song, Y., Tong, D., Zheng, B., Cui, H., Man, H., Zhang, Q. and He, K.: Anthropogenic emission inventories in China: a review, *National Science Review*, 4(6), 834–866, doi:10.1093/nsr/nwx150, 2017a.
- Li, M., Zhang, Q., Kurokawa, J.-I., Woo, J.-H., He, K., Lu, Z., Ohara, T., Song, Y., Streets, D. G., Carmichael, G. R., Cheng, Y., Hong, C., Huo, H., Jiang, X., Kang, S., Liu, F., Su, H. and Zheng, B.: MIX: a mosaic Asian anthropogenic emission inventory under the international collaboration framework of the MICS-Asia and HTAP, *Atmospheric Chemistry and Physics*, 17(2), 935–963, doi:10.5194/acp-17-935-2017, 2017b.
- 380 Lin, C. Q., Liu, G., Lau, A. K. H., Li, Y., Li, C. C., Fung, J. C. H. and Lao, X. Q.: High-resolution satellite remote sensing of provincial PM_{2.5} trends in China from 2001 to 2015, *Atmospheric Environment*, 180, 110–116, doi:10.1016/j.atmosenv.2018.02.045, 2018.
- 385 Lin, J., Nielsen, C. P., Zhao, Y., Lei, Y., Liu, Y. and McElroy, M. B.: Recent Changes in Particulate Air Pollution over China Observed from Space and the Ground: Effectiveness of Emission Control, *Environ. Sci. Technol.*, 44(20), 7771–7776, doi:10.1021/es101094t, 2010.
- Lin, J.-T. and McElroy, M. B.: Impacts of boundary layer mixing on pollutant vertical profiles in the lower troposphere: Implications to satellite remote sensing, *Atmospheric Environment*, 44(14), 1726–1739, doi:10.1016/j.atmosenv.2010.02.009, 390 2010.
- Lin, J.-T. and McElroy, M. B.: Detection from space of a reduction in anthropogenic emissions of nitrogen oxides during the Chinese economic downturn, *Atmospheric Chemistry and Physics*, 11(15), 8171–8188, doi:10.5194/acp-11-8171-2011, 2011.
- 395 Lin, J.-T., Martin, R. V., Boersma, K. F., Sneep, M., Stammes, P., Spurr, R., Wang, P., Van Roozendael, M., Clémer, K. and Irie, H.: Retrieving tropospheric nitrogen dioxide from the Ozone Monitoring Instrument: effects of aerosols, surface reflectance anisotropy, and vertical profile of nitrogen dioxide, *Atmospheric Chemistry and Physics*, 14(3), 1441–1461, doi:10.5194/acp-14-1441-2014, 2014.



- Lin, J.-T., Liu, M.-Y., Xin, J.-Y., Boersma, K. F., Spurr, R., Martin, R. and Zhang, Q.: Influence of aerosols and surface reflectance on satellite NO₂ retrieval: seasonal and spatial characteristics and implications for NO_x emission constraints, *Atmospheric Chemistry and Physics*, 15(19), 11217–11241, doi:10.5194/acp-15-11217-2015, 2015.
- 400 Lin, N., Wang, Y., Zhang, Y. and Yang, K.: A large decline of tropospheric NO₂ in China observed from space by SNPP OMPS, *Science of The Total Environment*, 675, 337–342, doi:10.1016/j.scitotenv.2019.04.090, 2019.
- Liu, F., Zhang, Q., van der A, R. J., Zheng, B., Tong, D., Yan, L., Zheng, Y. and He, K.: Recent reduction in NO_x emissions over China: synthesis of satellite observations and emission inventories, *Environmental Research Letters*, 11(11), 114002, doi:10.1088/1748-9326/11/11/114002, 2016.
- 405 Liu, F., Beirle, S., Zhang, Q., van der A, R. J., Zheng, B., Tong, D. and He, K.: NO_x emission trends over Chinese cities estimated from OMI observations during 2005 to 2015, *Atmospheric Chemistry and Physics*, 17(15), 9261–9275, doi:10.5194/acp-17-9261-2017, 2017.
- Liu, M., Lin, J., Boersma, K. F., Pinardi, G., Wang, Y., Chimot, J., Wagner, T., Xie, P., Eskes, H., Van Roozendaal, M., Hendrick, F., Wang, P., Wang, T., Yan, Y., Chen, L. and Ni, R.: Improved aerosol correction for OMI tropospheric NO₂ retrieval over East Asia: constraint from CALIOP aerosol vertical profile, *Atmospheric Measurement Techniques*, 12(1), 1–21, doi:10.5194/amt-12-1-2019, 2019.
- 415 Lorente, A., Folkert Boersma, K., Yu, H., Dörner, S., Hilboll, A., Richter, A., Liu, M., Lamsal, L. N., Barkley, M., De Smedt, I., Van Roozendaal, M., Wang, Y., Wagner, T., Beirle, S., Lin, J.-T., Krotkov, N., Stammes, P., Wang, P., Eskes, H. J. and Krol, M.: Structural uncertainty in air mass factor calculation for NO₂ and HCHO satellite retrievals, *Atmospheric Measurement Techniques*, 10(3), 759–782, doi:10.5194/amt-10-759-2017, 2017.
- Lu, Z. and Streets, D. G.: Increase in NO_x Emissions from Indian Thermal Power Plants during 1996–2010: Unit-Based Inventories and Multisatellite Observations, *Environ. Sci. Technol.*, 46(14), 7463–7470, doi:10.1021/es300831w, 2012.
- 420 Manders, A. M. M., Bultjes, P. J. H., Curier, L., Denier van der Gon, H. A. C., Hendriks, C., Jonkers, S., Kranenburg, R., Kuenen, J. J. P., Segers, A. J., Timmermans, R. M. A., Visschedijk, A. J. H., Wichink Kruit, R. J., van Pul, W. A. J., Sauter, F. J., van der Swaluw, E., Swart, D. P. J., Douros, J., Eskes, H., van Meijgaard, E., van Ulft, B., van Velthoven, P., Banzhaf, S., Mues, A. C., Stern, R., Fu, G., Lu, S., Heemink, A., van Velzen, N. and Schaap, M.: Curriculum vitae of the LOTOS–EUROS (v2.0) chemistry transport model, *Geoscientific Model Development*, 10(11), 4145–4173, doi:10.5194/gmd-10-4145-2017, 2017.
- 425 Martin, R. V.: Satellite remote sensing of surface air quality, *Atmospheric Environment*, 42(34), 7823–7843, doi:10.1016/j.atmosenv.2008.07.018, 2008.
- Martin, R. V., Jacob, D. J., Chance, K., Kurosu, T. P., Palmer, P. I. and Evans, M. J.: Global inventory of nitrogen oxide emissions constrained by space-based observations of NO₂ columns, *Journal of Geophysical Research: Atmospheres*, 108(D17), doi:10.1029/2003JD003453, 2003.
- 430 Menut, L., Bessagnet, B., Khvorostyanov, D., Beekmann, M., Blond, N., Colette, A., Coll, I., Curci, G., Foret, G., Hodzic, A., Mailler, S., Meleux, F., Monge, J.-L., Pison, I., Siour, G., Turquety, S., Valari, M., Vautard, R. and Vivanco, M. G.: CHIMERE 2013: a model for regional atmospheric composition modelling, *Geoscientific Model Development*, 6(4), 981–1028, doi:10.5194/gmd-6-981-2013, 2013.



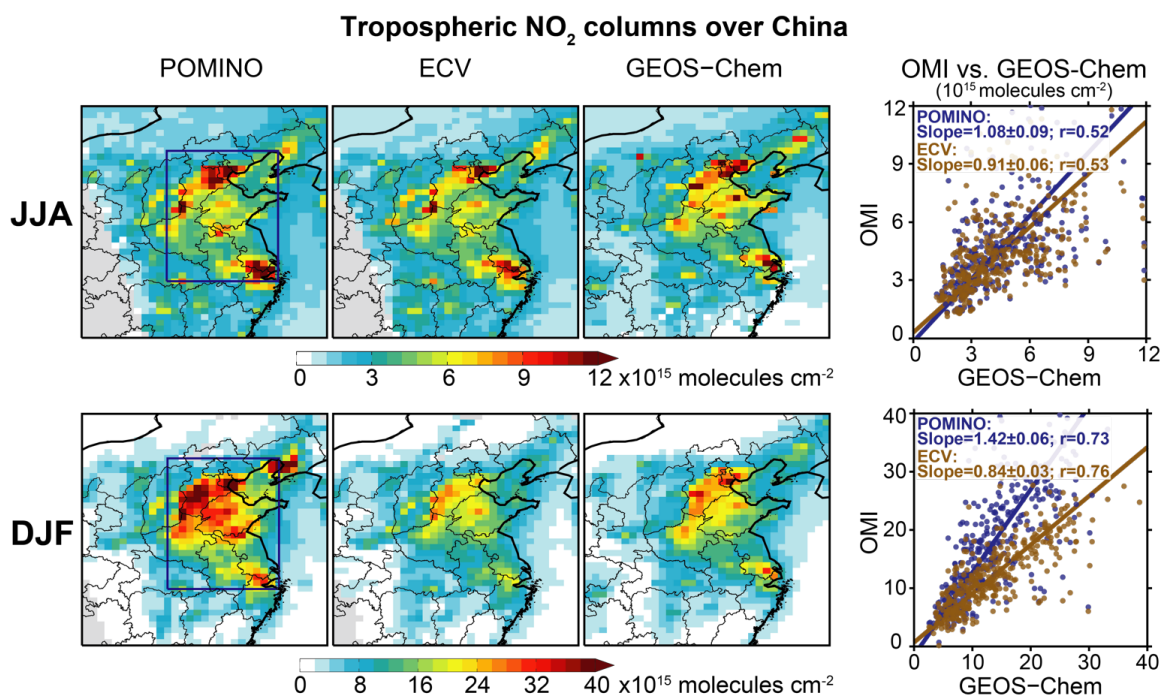
- Miao, R., Chen, Q., Sun, Y. L. and Guo, J. P.: Seasonal Variations of Model Bias in Simulations of Major PM_{2.5} Chemical Components in China, Xi'an China., 2018.
- 435 Murray, L. T., Jacob, D. J., Logan, J. A., Hudman, R. C. and Koshak, W. J.: Optimized regional and interannual variability of lightning in a global chemical transport model constrained by LIS/OTD satellite data, *Journal of Geophysical Research: Atmospheres*, 117(D20), doi:10.1029/2012JD017934, 2012.
- Palmer, P. I., Jacob, D. J., Chance, K., Martin, R. V., Spurr, R. J. D., Kurosu, T. P., Bey, I., Yantosca, R., Fiore, A. and Li, Q.: Air mass factor formulation for spectroscopic measurements from satellites: Application to formaldehyde retrievals from the
440 Global Ozone Monitoring Experiment, *Journal of Geophysical Research: Atmospheres*, 106(D13), 14539–14550, doi:10.1029/2000JD900772, 2001.
- Pye, H. O. T., Liao, H., Wu, S., Mickley, L. J., Jacob, D. J., Henze, D. K. and Seinfeld, J. H.: Effect of changes in climate and emissions on future sulfate-nitrate-ammonium aerosol levels in the United States, *Journal of Geophysical Research*, 114(D1), doi:10.1029/2008JD010701, 2009.
- 445 Richter, A., Burrows, J. P., Nüß, H., Granier, C. and Niemeier, U.: Increase in tropospheric nitrogen dioxide over China observed from space, *Nature*, 437, 129, 2005.
- Saikawa, E., Kim, H., Zhong, M., Avramov, A., Zhao, Y., Janssens-Maenhout, G., Kurokawa, J.-I., Klimont, Z., Wagner, F., Naik, V., Horowitz, L. W. and Zhang, Q.: Comparison of emissions inventories of anthropogenic air pollutants and greenhouse gases in China, *Atmospheric Chemistry and Physics*, 17(10), 6393–6421, doi:10.5194/acp-17-6393-2017, 2017.
- 450 Schneider, P., Lahoz, W. A. and van der A, R.: Recent satellite-based trends of tropospheric nitrogen dioxide over large urban agglomerations worldwide, *Atmospheric Chemistry and Physics*, 15(3), 1205–1220, doi:10.5194/acp-15-1205-2015, 2015.
- Shah, V., Jaeglé, L., Thornton, J. A., Lopez-Hilfiker, F. D., Lee, B. H., Schroder, J. C., Campuzano-Jost, P., Jimenez, J. L., Guo, H., Sullivan, A. P., Weber, R. J., Green, J. R., Fiddler, M. N., Bililign, S., Campos, T. L., Stell, M., Weinheimer, A. J., Montzka, D. D. and Brown, S. S.: Chemical feedbacks weaken the wintertime response of particulate sulfate and nitrate to
455 emissions reductions over the eastern United States, *Proceedings of the National Academy of Sciences*, 115(32), 8110, doi:10.1073/pnas.1803295115, 2018.
- Sherwen, T., Schmidt, J. A., Evans, M. J., Carpenter, L. J., Gros smann, K., Eastham, S. D., Jacob, D. J., Dix, B., Koenig, T. K., Sinreich, R., Ortega, I., Volkamer, R., Saiz-Lopez, A., Prados-Roman, C., Mahajan, A. S. and Ordóñez, C.: Global impacts of tropospheric halogens (Cl, Br, I) on oxidants and composition in GEOS-Chem, *Atmospheric Chemistry and Physics*, 16(18),
460 12239–12271, doi:10.5194/acp-16-12239-2016, 2016.
- Silvern, R. F., Jacob, D. J., Mickley, L. J., Sulprizio, M. P., Travis, K. R., Marais, E. A., Cohen, R. C., Laughner, J. L., Choi, S., Joiner, J. and Lamsal, L. N.: Using satellite observations of tropospheric NO₂ columns to infer long-term trends in US NO_x emissions: the importance of accounting for the free tropospheric NO₂ background, *Atmospheric Chemistry and Physics*, 19(13), 8863–8878, doi:10.5194/acp-19-8863-2019, 2019.
- 465 Spataro, F., Ianniello, A., Esposito, G., Allegrini, I., Zhu, T. and Hu, M.: Occurrence of atmospheric nitrous acid in the urban area of Beijing (China), *Science of The Total Environment*, 447, 210–224, doi:10.1016/j.scitotenv.2012.12.065, 2013.
- Stavrakou, T., Müller, J.-F., Boersma, K. F., De Smedt, I. and van der A, R. J.: Assessing the distribution and growth rates of NO_x emission sources by inverting a 10-year record of NO₂ satellite columns, *Geophysical Research Letters*, 35(10), doi:10.1029/2008GL033521, 2008.



- 470 Stemmler, K., Ndour, M., Elshorbany, Y., Kleffmann, J., D'Anna, B., George, C., Bohn, B. and Ammann, M.: Light induced conversion of nitrogen dioxide into nitrous acid on submicron humic acid aerosol, *Atmospheric Chemistry and Physics*, 7(16), 4237–4248, doi:10.5194/acp-7-4237-2007, 2007.
- Stettler, M. E. J., Eastham, S. and Barrett, S. R. H.: Air quality and public health impacts of UK airports. Part I: Emissions, *Atmospheric Environment*, 45(31), 5415–5424, doi:10.1016/j.atmosenv.2011.07.012, 2011.
- 475 Streets, D. G., Canty, T., Carmichael, G. R., de Foy, B., Dickerson, R. R., Duncan, B. N., Edwards, D. P., Haynes, J. A., Henze, D. K., Houyoux, M. R., Jacob, D. J., Krotkov, N. A., Lamsal, L. N., Liu, Y., Lu, Z., Martin, R. V., Pfister, G. G., Pinder, R. W., Salawitch, R. J. and Wecht, K. J.: Emissions estimation from satellite retrievals: A review of current capability, *Atmospheric Environment*, 77, 1011–1042, doi:10.1016/j.atmosenv.2013.05.051, 2013.
- Sun, W., Shao, M., Granier, C., Liu, Y., Ye, C. S. and Zheng, J. Y.: Long-Term Trends of Anthropogenic SO₂, NO_x, CO, and NMVOCs Emissions in China, *Earth's Future*, 6(8), 1112–1133, doi:10.1029/2018EF000822, 2018.
- Tan, F., Tong, S., Jing, B., Hou, S., Liu, Q., Li, K., Zhang, Y. and Ge, M.: Heterogeneous reactions of NO₂ with CaCO₃–(NH₄)₂SO₄ mixtures at different relative humidities, *Atmospheric Chemistry and Physics*, 16(13), 8081–8093, doi:10.5194/acp-16-8081-2016, 2016.
- 485 Tan, Z., Rohrer, F., Lu, K., Ma, X., Bohn, B., Broch, S., Dong, H., Fuchs, H., Gkatzelis, G. I., Hofzumahaus, A., Holland, F., Li, X., Liu, Y., Liu, Y., Novelli, A., Shao, M., Wang, H., Wu, Y., Zeng, L., Hu, M., Kiendler-Scharr, A., Wahner, A. and Zhang, Y.: Wintertime photochemistry in Beijing: observations of RO_x radical concentrations in the North China Plain during the BEST-ONE campaign, *Atmospheric Chemistry and Physics*, 18(16), 12391–12411, doi:10.5194/acp-18-12391-2018, 2018.
- 490 Travis, K. R., Jacob, D. J., Fisher, J. A., Kim, P. S., Marais, E. A., Zhu, L., Yu, K., Miller, C. C., Yantosca, R. M., Sulprizio, M. P., Thompson, A. M., Wennberg, P. O., Crounse, J. D., St. Clair, J. M., Cohen, R. C., Laughner, J. L., Dibb, J. E., Hall, S. R., Ullmann, K., Wolfe, G. M., Pollack, I. B., Peischl, J., Neuman, J. A. and Zhou, X.: Why do models overestimate surface ozone in the Southeast United States?, *Atmospheric Chemistry and Physics*, 16(21), 13561–13577, doi:10.5194/acp-16-13561-2016, 2016.
- 495 Uno, I., He, Y., Ohara, T., Yamaji, K., Kurokawa, J.-I., Katayama, M., Wang, Z., Noguchi, K., Hayashida, S., Richter, A. and Burrows, J. P.: Systematic analysis of interannual and seasonal variations of model-simulated tropospheric NO₂ in Asia and comparison with GOME-satellite data, *Atmospheric Chemistry and Physics*, 7(6), 1671–1681, doi:10.5194/acp-7-1671-2007, 2007.
- Valin, L. C., Russell, A. R., Hudman, R. C. and Cohen, R. C.: Effects of model resolution on the interpretation of satellite NO₂ observations, *Atmospheric Chemistry and Physics*, 11(22), 11647–11655, doi:10.5194/acp-11-11647-2011, 2011.
- 500 van der A, R. J., Peters, D. H. M. U., Eskes, H., Boersma, K. F., Van Roozendaal, M., De Smedt, I. and Kelder, H. M.: Detection of the trend and seasonal variation in tropospheric NO₂ over China, *Journal of Geophysical Research: Atmospheres*, 111(D12), doi:10.1029/2005JD006594, 2006.
- 505 van der A, R. J., Eskes, H. J., Boersma, K. F., van Noije, T. P. C., Van Roozendaal, M., De Smedt, I., Peters, D. H. M. U. and Meijer, E. W.: Trends, seasonal variability and dominant NO_x source derived from a ten year record of NO₂ measured from space, *Journal of Geophysical Research: Atmospheres*, 113(D4), doi:10.1029/2007JD009021, 2008.



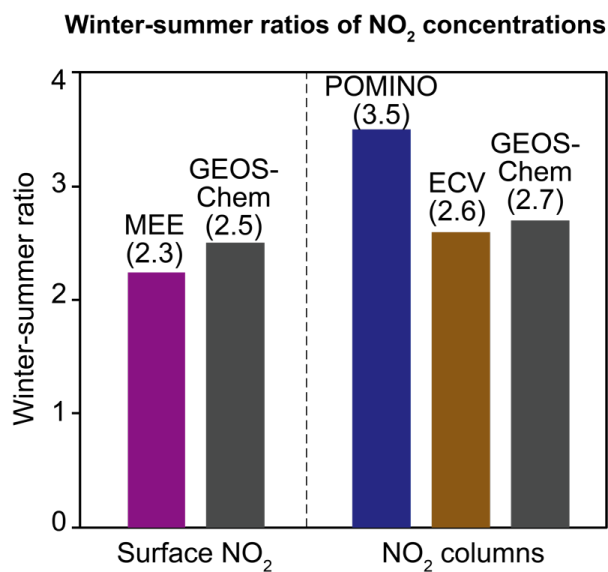
- Vinken, G. C. M., Boersma, K. F., Jacob, D. J. and Meijer, E. W.: Accounting for non-linear chemistry of ship plumes in the GEOS-Chem global chemistry transport model, *Atmospheric Chemistry and Physics*, 11(22), 11707–11722, doi:10.5194/acp-11-11707-2011, 2011.
- 510 Wang, J., Zhang, X., Guo, J., Wang, Z. and Zhang, M.: Observation of nitrous acid (HONO) in Beijing, China: Seasonal variation, nocturnal formation and daytime budget, *Science of The Total Environment*, 587–588, 350–359, doi:10.1016/j.scitotenv.2017.02.159, 2017.
- Wang, S., Zhou, R., Zhao, H., Wang, Z., Chen, L. and Zhou, B.: Long-term observation of atmospheric nitrous acid (HONO) and its implication to local NO₂ levels in Shanghai, China, *Atmospheric Environment*, 77, 718–724, doi:10.1016/j.atmosenv.2013.05.071, 2013.
- 515 Wang, Y. X., McElroy, M. B., Jacob, D. J. and Yantosca, R. M.: A nested grid formulation for chemical transport over Asia: Applications to CO: Nested grid CO simulation over Asia, *Journal of Geophysical Research: Atmospheres*, 109(D22), doi:10.1029/2004JD005237, 2004.
- Zhai, S., Jacob, D. J., Wang, X., Shen, L., Li, K., Zhang, Y., Gui, K., Zhao, T. and Liao, H.: Fine particulate matter (PM_{2.5}) trends in China, 2013–2018: contributions from meteorology, *Atmospheric Chemistry and Physics Discussions*, 2019, 1–19, doi:10.5194/acp-2019-279, 2019.
- 520 Zhang, L., Jacob, D. J., Knipping, E. M., Kumar, N., Munger, J. W., Carouge, C. C., van Donkelaar, A., Wang, Y. X. and Chen, D.: Nitrogen deposition to the United States: distribution, sources, and processes, *Atmospheric Chemistry and Physics*, 12(10), 4539–4554, doi:10.5194/acp-12-4539-2012, 2012a.
- Zhang, Q., Streets, D. G., He, K., Wang, Y., Richter, A., Burrows, J. P., Uno, I., Jang, C. J., Chen, D., Yao, Z. and Lei, Y.: NO_x emission trends for China, 1995–2004: The view from the ground and the view from space, *Journal of Geophysical Research: Atmospheres*, 112(D22), doi:10.1029/2007JD008684, 2007.
- Zhang, Q., Geng, G., Wang, S., Richter, A. and He, K.: Satellite remote sensing of changes in NO_x emissions over China during 1996–2010, *Chinese Science Bulletin*, 57(22), 2857–2864, doi:10.1007/s11434-012-5015-4, 2012b.
- 530 Zheng, B., Tong, D., Li, M., Liu, F., Hong, C., Geng, G., Li, H., Li, X., Peng, L., Qi, J., Yan, L., Zhang, Y., Zhao, H., Zheng, Y., He, K. and Zhang, Q.: Trends in China's anthropogenic emissions since 2010 as the consequence of clean air actions, *Atmospheric Chemistry and Physics*, 18(19), 14095–14111, doi:10.5194/acp-18-14095-2018, 2018.



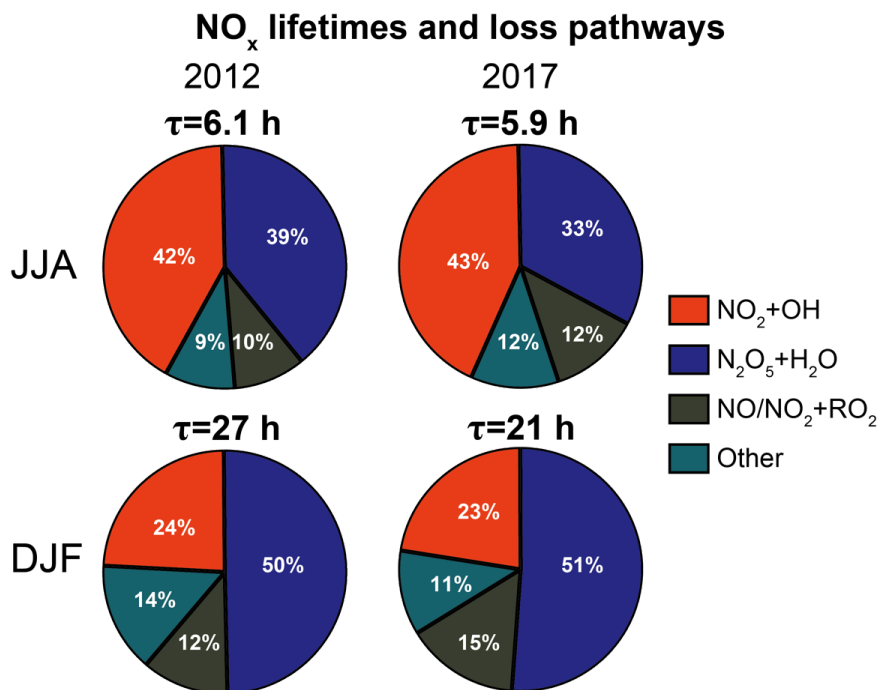
535

540

Figure 1: Tropospheric NO₂ columns over China. Values are 3-month means for June-July-August (JJA) 2017 and December-January-February (DJF) 2016/17 on the 0.5°×0.625° GEOS-Chem grid. OMI retrievals from POMINO (Liu et al., 2019) and ECV (Boersma et al., 2018) are compared with the GEOS-Chem model. The JJA and DJF panels have different color scales. Locations where none of the OMI data met our selection criteria are in grey. The scatterplots show the spatial correlations between the OMI retrievals and GEOS-Chem on the 0.5°×0.625° grid for central-eastern China (delineated box in left panels), along with the Pearson's correlation coefficient (*r*), reduced-major-axis linear regressions, and regression slopes. Error standard deviations on the slopes were derived by the bootstrap method.



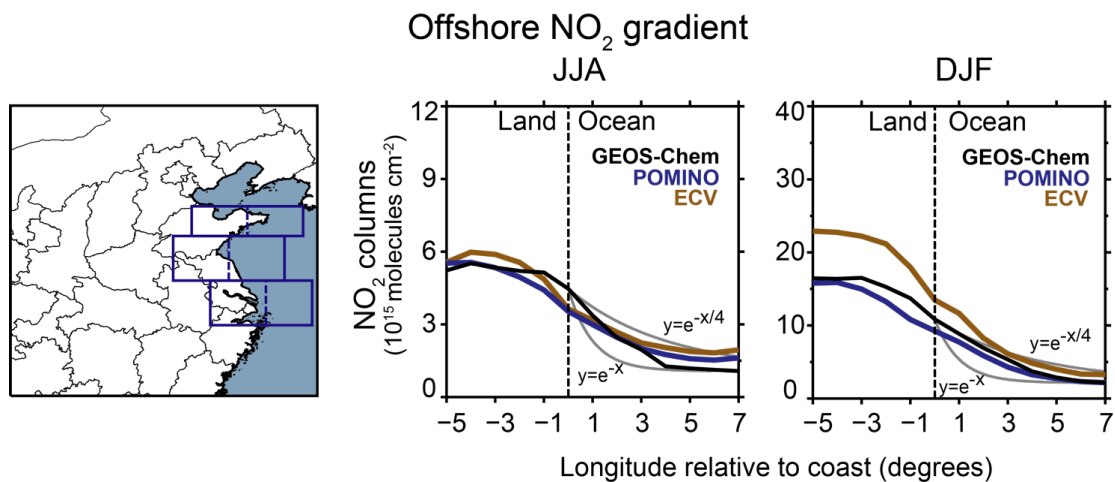
545 **Figure 2:** Mean winter-summer ratios of NO₂ concentrations over central-eastern China. The values are ratios of the seasonal mean NO₂ surface concentrations observed at the ensemble of MEE sites in central-eastern China, and of the mean POMINO and ECV tropospheric NO₂ columns (recalculated using the GEOS-Chem NO₂ profiles) at the MEE station locations. Central-eastern China is as defined by the rectangle in Figure 1. GEOS-Chem values sampled at the measurement locations are also shown. Observations and model results are for JJA 2017 (summer) and DJF 2016/17 (winter).



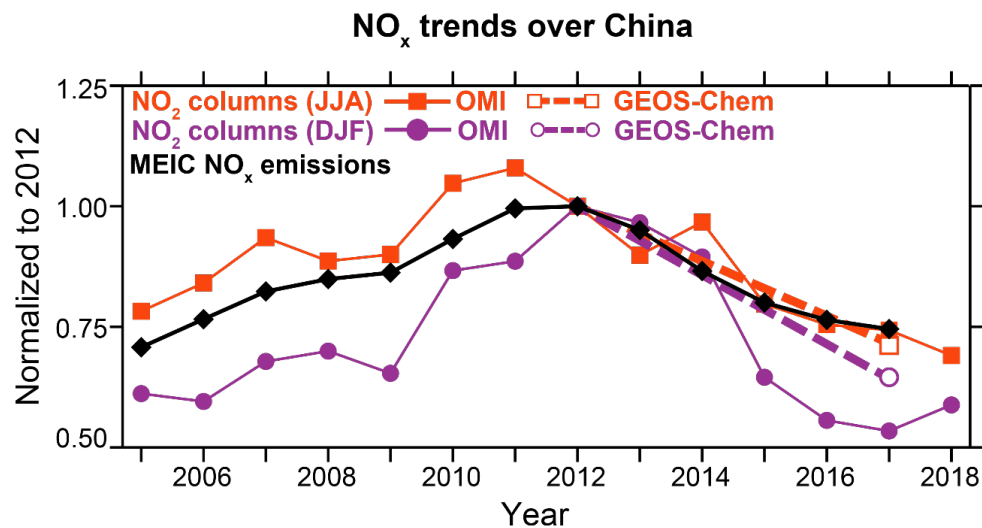
550

Figure 3: NO_x lifetime (τ) and loss pathways in the boundary layer over central-eastern China. The lifetimes are the GEOS-Chem averages for the bottom 0-2 km of atmosphere over the domain delineated in Figure 1, and the pie charts show the relative contributions of the different NO_x sinks. For the lifetime calculation we define NO_x as NO+NO₂+NO₃+2N₂O₅+HONO+HNO₄+ClNO₂. Values are given for summer (JJA) and winter (DJF) of 2012 and 2017. The sink from NO/NO₂+RO₂ is the net flux, accounting for partial recycling of the organic nitrates, and includes the contributions from peroxyacyl nitrates (PANs). The 'Other' sinks include NO₃+VOC reactions, NO₂ and NO₃ hydrolysis in aerosols, and NO_x deposition.

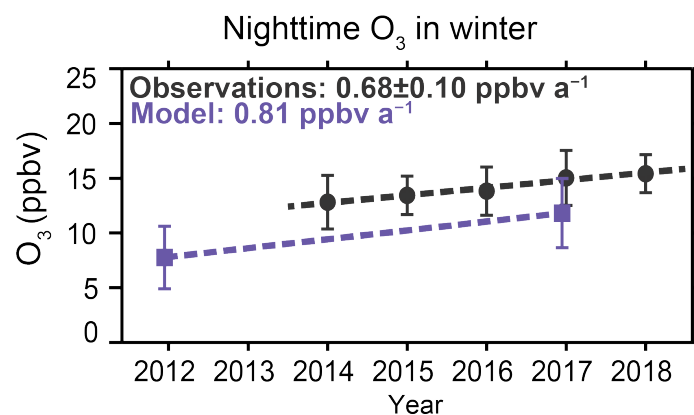
555



560 **Figure 4: Offshore gradient of NO_2 .** The right panels show the seasonal-mean longitudinal gradient of OMI and GEOS-Chem columns across China's eastern coast averaged over the latitudinal sections marked in the left panel. The dashed lines indicate approximate land-ocean boundaries. The decay curves corresponding to e-folding lengths of 1° and 4° longitude are also shown.



565 Figure 5: Trends in NO_x emissions and NO₂ concentrations over central-eastern China. The figure shows the JJA and DJF relative trends in the OMI (ECV) tropospheric NO₂ columns averaged over central-eastern China (domain delineated in Figure 1) for the 2004–2018 duration of the OMI record, and the corresponding trends in annual NO_x emissions estimated by the MEIC inventory. GEOS-Chem 2012–2017 trends in NO₂ columns are also shown. All quantities are normalized to a value of 1 in 2012.



570 **Figure 6:** Trend in nighttime surface ozone in China in winter. Values are DJF means over 21:00–5:00 local time for the network of sites in central-eastern China operated since 2013 by the China Ministry of Ecology and Environment (MEE). The sites are gridded on the 0.5°×0.625° GEOS-Chem grid. The symbols are averages for all grid cells containing sites and vertical bars are the standard deviation of the spatial distribution. Model values are similarly sampled and gridded over the ensemble of MEE sites operating since 2013. Trends are from an ordinary least squares regression.